Natural convection in an enclosure with partially active walls is studied by Nithyadevi et al. [13, 14] and Kandaswamy et al. [15] without Soret and Dufour effects. Present study deals with the natural convection in a square enclosure filled with water and partially heated vertical walls for three different combinations of heating location in the presence of solute concentration with Soret and Dufour effects. The hot region is located at the top, middle and bottom of the left vertical wall of the enclosure.

Oztop and Abu-Nada [16] numerically studied natural convection in partially heated rectangular enclosures filled with nanofluids. Rouboa et al. [17] analyzed convective heat transfer in nanofluid. Esfahani and Bordbar [18] studied double diffusive natural convection heat transfer enhancement in a square enclosure using nanofluids. Gorla et al. [19] analyzed mixed convective boundary layer flow over a vertical wedge embedded in a porous medium saturated with a nanofluid: Natural Convection Dominated Regime. Kuznetsov and Nield [20] performed double-diffusive natural convective boundary-layer flow of a nanofluid past a vertical plate where similarity solution was performed in order to obtain correlation formulas giving the reduced Nusselt number as a function of the various relevant parameters. At the same year, Nield and Kuznetsov [21, 22] conducted the onset of double-diffusive convection in a nanofluid layer and the Cheng–Minkowycz problem for the double-diffusive natural convective boundary layer flow in a porous medium saturated by a nanofluid. The stability boundaries for both non-oscillatory and oscillatory cases had been approximated by simple analytical expressions. For the porous medium the Darcy model is employed.

Effects of Soret Dufour, chemical reaction and thermal radiation on MHD non-Darcy unsteady mixed convective heat and mass transfer over a stretching sheet was investigated by Pal and Mondal [23]. The author used shooting algorithm with Runge–Kutta–Fehlberg integration scheme to solve the governing equations. Natural convection heat transfer of nanofluids in a vertical cavity: Effects of non-uniform particle diameter and temperature on thermal conductivity was performed by Lin and Violi [24]. Moreover, Saleh et al. [25] studied natural convection heat transfer in a nanofluid-filled trapezoidal enclosure. They found that acute sloping wall and Cu nanoparticles with high concentration were effective to enhance the rate of heat transfer.

## 2. FORMULATION OF PROBLEM

Fig. 1 shows a schematic diagram of a partially heated square enclosure. The fluid in the cavity is water-based nanofluid containing $Al_2O_3$ nanoparticles with Soret and Dufour coefficients. The nanofluid is assumed incompressible and the flow is considered to be laminar. It is taken that water and nanoparticles are in thermal equilibrium and no slip occurs between them. The top horizontal wall has constant temperature $T_c$, while bottom wall is partially heated $T_h$, with $T_h > T_c$. The concentration in top wall is maintained higher than bottom wall ($C_c < C_h$). The remaining bottom wall and the two vertical walls are considered adiabatic. The thermophysical properties of the nanofluid are taken from Saleh et al. [25] and given in Table 1. The density of the nanofluid is approximated by the Boussinesq model.

The governing equations for laminar natural convection in a solar collector filled with water-alumina nanofluid in terms of the Navier-Stokes and energy equation (dimensional form) are given as:

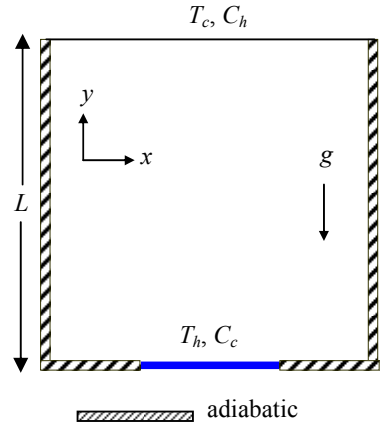


Fig. 1: Schematic diagram of the enclosure

Continuity equation:

$$\frac{\partial u}{\partial x}+\frac{\partial v}{\partial y}=0 \tag{1}$$

$x$-momentum equation:

$$\rho_{nf}\left(u\frac{\partial u}{\partial x}+v\frac{\partial u}{\partial y}\right)=-\frac{\partial p}{\partial x}+\mu_{nf}\left(\frac{\partial^2 u}{\partial x^2}+\frac{\partial^2 u}{\partial y^2}\right) \tag{2}$$

y-momentum equation:

$$\rho_{nf}\left(u\frac{\partial v}{\partial x}+v\frac{\partial v}{\partial y}\right)=-\frac{\partial p}{\partial y}+\mu_{nf}\left(\frac{\partial^2 v}{\partial x^2}+\frac{\partial^2 v}{\partial y^2}\right)+ g\rho_{nf}\beta_{nf}\left\{(T-T_c)-(c-C_c)\right\} \tag{3}$$

Energy equation:

$$u\frac{\partial T}{\partial x}+v\frac{\partial T}{\partial y}=\alpha_{nf}\left(\frac{\partial^2 T}{\partial x^2}+\frac{\partial^2 T}{\partial y^2}\right)+\frac{DK_{Tf}}{C_sC_p}\left(\frac{\partial^2 c}{\partial x^2}+\frac{\partial^2 c}{\partial y^2}\right) \tag{4}$$

Concentration equation:

$$u\frac{\partial c}{\partial x}+v\frac{\partial c}{\partial y}=\alpha_{nf}\left(\frac{\partial^2 c}{\partial x^2}+\frac{\partial^2 c}{\partial y^2}\right)+\frac{DK_{Tf}}{T_m}\left(\frac{\partial^2 T}{\partial x^2}+\frac{\partial^2 T}{\partial y^2}\right) \tag{5}$$

The boundary conditions are:

at all solid boundaries $u = v = 0$
at $y = 0,\ 0.3 \le x \le 0.7,\quad T = T_h,\ c = C_c$
at $y = 1,\quad T = T_c,\ c = C_h$
at the remaining boundaries $\frac{\partial T}{\partial n}=0,\ \frac{\partial c}{\partial n}=0$

where, $\rho_{nf}=(1-\phi)\rho_f+\phi\rho_s$ is the density,

$(\rho C_p)_{nf}=(1-\phi)(\rho C_p)_f+\phi(\rho C_p)_s$ is the heat capacitance,

$\beta_{nf}=(1-\phi)\beta_f+\phi\beta_s$ is the thermal expansion coefficient,

$\alpha_{nf}=k_{nf}/(\rho C_p)_{nf}$ is the thermal diffusivity,

the dynamic viscosity of Brinkman model [26] is $\mu_{nf}=\mu_f(1-\phi)^{-2.5}$

and the thermal conductivity of Maxwell Garnett (MG) model [27] is $k_{nf}=k_f\dfrac{k_s+2k_f-2\phi(k_f-k_s)}{k_s+2k_f+\phi(k_f-k_s)}$.

To make the above equations non-dimensionalized we use the following dimensionless dependent and independent variables:

$$X=\frac{x}{L},\quad Y=\frac{y}{L},\quad U=\frac{uL}{\nu_f},\quad V=\frac{vL}{\nu_f},$$

$$P=\frac{pL^2}{\rho_f \nu_f{}^2},\quad \theta=\frac{T-T_c}{T_h-T_c},\quad C=\frac{c-C_c}{C_h-C_c}$$

The obtained dimensionless form of t he governing equations are:

$$\frac{\partial U}{\partial X}+\frac{\partial V}{\partial Y}=0 \tag{6}$$

$$U\frac{\partial U}{\partial X}+V\frac{\partial U}{\partial Y}=-\frac{\rho_f}{\rho_{nf}}\frac{\partial P}{\partial X}+Pr\frac{\nu_{nf}}{\nu_f}\left(\frac{\partial^2 U}{\partial X^2}+\frac{\partial^2 U}{\partial Y^2}\right) \tag{7}$$

$$U\frac{\partial V}{\partial X}+V\frac{\partial V}{\partial Y}=-\frac{\rho_f}{\rho_{nf}}\frac{\partial P}{\partial Y}+Pr\frac{\nu_{nf}}{\nu_f}\left(\frac{\partial^2 V}{\partial X^2}+\frac{\partial^2 V}{\partial Y^2}\right)+ Ra\,Pr\frac{(1-\phi)\rho_f\beta_f+\phi\rho_s\beta_s}{\rho_{nf}\beta_f}(\theta-Nr\,C) \tag{8}$$

$$U\frac{\partial \theta}{\partial X}+V\frac{\partial \theta}{\partial Y}=\frac{1}{Pr}\left(\frac{\partial^2 \theta}{\partial X^2}+\frac{\partial^2 \theta}{\partial Y^2}\right)+D_f\left(\frac{\partial^2 C}{\partial X^2}+\frac{\partial^2 C}{\partial Y^2}\right) \tag{9}$$

$$U\frac{\partial C}{\partial X}+V\frac{\partial C}{\partial Y}=\frac{1}{Sc}\left(\frac{\partial^2 C}{\partial X^2}+\frac{\partial^2 C}{\partial Y^2}\right)+S_r\left(\frac{\partial^2 \theta}{\partial X^2}+\frac{\partial^2 \theta}{\partial Y^2}\right) \tag{10}$$

Here $Pr=\left(\frac{\nu}{\alpha}\right)_f$ is the Prandtl number, $Sc=\left(\frac{\nu}{D}\right)_f$ is the Schmidt number, $Ra=\frac{g\beta_f L^3(T_h-T_c)}{\nu_f\alpha_f}$ is th e Rayleigh number, $Ra_T=\frac{g\beta_{Tf} L^3(T_h-T_c)}{\nu_f\alpha_f}$ is the thermal Rayleigh number, $Ra_c=\frac{g\beta_{cf} L^3(C_h-C_c)}{\nu_f\alpha_f}$ is the solutal Rayleigh number, $N=\frac{Ra_c}{Ra_T}$ is the buoyancy ratio number, $D_f=\left(\frac{D}{\nu}\right)_f\frac{k_{Tf}(C_h-C_c)}{C_sC_p(T_h-T_c)}$ is the Dufour and $S_r=\left(\frac{D}{\nu}\right)_f\frac{k_{Tf}(T_h-T_c)}{T_m(C_h-C_c)}$ is the Soret coefficient.

The corresponding boundary conditions take the following form:

at all solid boundaries $U=V=0$

at $Y=0,\ 0.3\le X\le 0.7,\quad \theta=1,\ C=0$

at $Y=1,\quad \theta=0,\ C=1$

at the remaining boundaries $\frac{\partial\theta}{\partial N}=0,\ \frac{\partial C}{\partial N}=0$

The average Nusselt and Sherwood numbers at the heated and concentrated surfaces of the enclosure may be expressed, respectively as

$$Nu=-\frac{1}{L_s}\int_0^{L_s}\frac{k_{nf}}{k_f}\frac{\partial\theta}{\partial Y}dX \quad\text{and}\quad Sh=-\int_0^1\frac{k_{nf}}{k_f}\frac{\partial C}{\partial Y}dX$$

The mean bulk temperature and concent ration of the working fluid inside the c avity may be writ ten as $\theta_{av}=\int\theta\,d\bar{V}/\bar{V}$ and $C_{av}=\int C\,d\bar{V}/\bar{V}$, where $\bar{V}$ is the volume of the enclosure.

Table 1: Thermo physical properties of fluid and nanoparticles [25]

| Physical Properties | Fluid phase (Water) | $Al_2O_3$ |
|---|---|---|
| $C_p$(J/kgK) | 4179 | 765 |
| $\rho$ (kg/m$^3$) | 997.1 | 3600 |
| $k$ (W/mK) | 0.6 | 46 |
| $\beta\times10^{-5}$ (1/K) | 21 | 0.63 |

## 3. NUMERICAL PROCEDURE

The Galerkin finite element method [28, 29] is used to solve the non-di mensional governing equations along with boundary conditions for the considered problem. The equation of cont inuity has bee n used as a constraint due to mass conservation and this restriction may be used to find the pressure distribution. The penalty finite element method [30] is used to s olve the Eqs. (2) - (4), where the pressure $P$ is eliminated by a penalty constraint. The continuity equation is automatically fulfilled for large values of this penalty constraint. Then the velocity components ($U$, $V$), temperature ($\theta$) and concentration ($C$) are expanded using a basis set. The Galerkin finite element technique yields the subsequent nonlinear residual equations. Three points Gaussian quadrature is used to evaluate the integrals in these equations. The non-linear residual equations are solved using Newt on–Raphson method to determine the coefficients of t he expansions. The convergence of sol utions is assumed when the relative error for e ach variable between consecutive iterations is recorded below the convergence criterion $\varepsilon$ such that $\left|\psi^{n+1}-\psi^{n}\right|\le 10^{-4}$, where $n$ is the number of iteration and $\Psi$ is a function of $U$, $V$, $\theta$ and $C$.

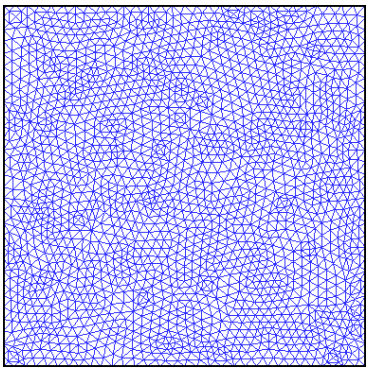

Fig. 2: Mesh generation of the cavity

Table 2: Grid Sensitivity Check at $Pr = 6.2$, $D_f = S_r = 0.5$, $Sc = 5$, $\phi = 5\%$ and $Ra = 10^4$

| Nodes (elements) | 6224 ( 2569) | 10982 ( 4730) | 13538 ( 6516) | 20295 ( 8457) | 27524 ( 10426) |
|---|---|---|---|---|---|
| *Nu* | 1.82945 | 3.18176 | 3.98701 | 4.420435 | 4.490436 |
| *Sh* | 0.12945 | 0.68176 | 0.98701 | 1.173416 | 1.193416 |
| Time (s) | 226.265 | 292.594 | 388.157 | 421.328 | 627.375 |

### 3.1 Mesh Generation

In the finite element method, the mesh generation is the technique to subdivide a domain into a set of sub-domains, called finite elements, control volume, etc. The discrete locations are defined by the numerical grid, at which the variables are to be calculated. It is basically a discrete representation of the geometric domain on which the problem is to be solved. The computational domains with irregular geometries by a collection of finite elements make the method a valuable practical tool for the solution of boundary value problems arising in various fields of engineering. Fig. 2 displays the finite element mesh of the present physical domain.

### 3.2 Grid Independent Test

An extensive mesh testing procedure is conducted to guarantee a grid-independent solution for $Ra = 10^4$, $Pr = 6.2$, $D_f = S_r = 0.5$, $Sc = 5$, $\phi = 5\%$ in the chamber. In the present work, we examine five different non-uniform grid systems with the following number of elements within the resolution field: 2569, 4730, 6516, 8457 and 10426. The numerical scheme is carried out for highly precise key in the average Nusselt (*Nu*) and Sherwood (*Sh*) numbers for the aforesaid elements to develop an understanding of the grid fineness as shown in Table 2 and Fig. 3. The scale of the average Nusselt and Sherwood numbers for 8457 elements shows a little difference with the results obtained for the other elements. Hence, considering the non-uniform grid system of 8457 elements is preferred for the computation.

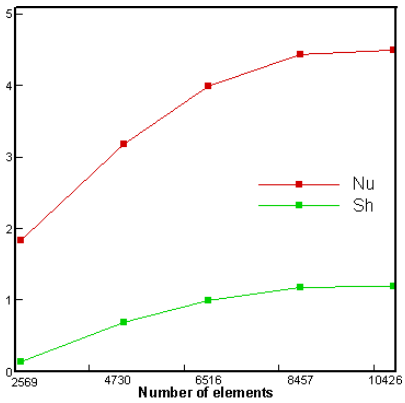


Fig. 3: Grid test for the geometry

### 3.3 Comparison

The present numerical solution is validated by comparing the current code results for streamlines, isotherms and concentration profiles using $D_f = S_r = 0.5$, $Sc = 5$, $Pr = 11.573$ and $Ra_T = 10^5$ with the graphical representation of Nithyadevi and Yang [2] which was reported for double diffusive natural convection in a partially heated enclosure with Soret and Dufour effects. Fig. 4 demonstrates the above stated comparison. As shown in Fig. 4, the numerical solutions (present work and Nithyadevi and Yang [2]) are in good agreement.

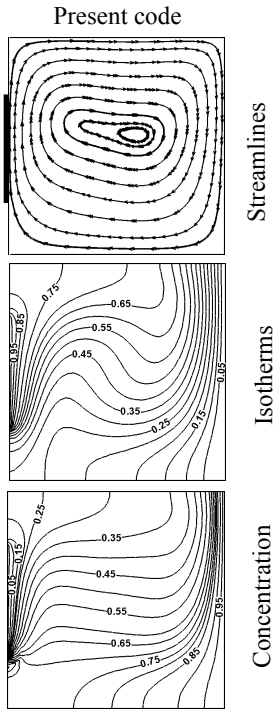


Fig. 4: Comparison between present work and Nithyadevi and Yang using [2] $R = 0.5$, $N = 1$, $D_f = S_r = 0.5$, $Sc = 5$ and $Ra_T = 10^5$

## 4. RESULTS AND DISCUSSION

In this section, numerical results of streamlines and isotherms for various values of Soret ($S_r$) and Dufour ($D_r$) coefficients and the Schmidt number ($Sc$) with $Al_2O_3$ /water nanofluid in a square enclosure are displayed. $Ra = Ra_T = Ra_c$ is assumed for the present numerical calculation. The considered values of $D_f$, $S_r$, $Sc$ are $D_f$ = (0, 0.5 and 1) = $S_r$ and $Sc$ (= 1, 3 and 5). But the Prandtl number $Pr = 6.2$, the Rayleigh number $Ra = 10^4$ and solid volume fraction of the nanofluid $\phi = 5\%$ are kept fixed for this study. In addition, the values of the average Nusselt and Sherwood numbers, mean temperature and concentration as well as horizontal and vertical velocities at the middle of the cavity have been calculated for different mentioned parameters.

Fig. 5 (a) - (c ) exposes the effect of $S_r$ on the flow, thermal and concentration fields while $D_f = 0.5$ and $Sc = 5$. At the absence of the Soret coefficient ($S_r$) a primary anticlockwise circulating cell occupies the bulk of the chamber. The size of the inner vortex of this cell becomes larger with the increasing of the Soret coefficient. In addition

for the largest value of $S_r$, the streamlines form rectangular pattern whereas initially they are circular. As well as another vortex is appeared near the left wall of the chamber. The isotherms and iso-concentrations are crowded around the active location on the bottom surface of the enclosure for ($S_r$ = 1). In addition, the temperature lines corresponding to $S_r$ = 1 become less bended. Decreasing Soret effect leads to deformation of the thermal and concentration boundary layers at the right part of the cold upper wall and middle of the bottom surface.

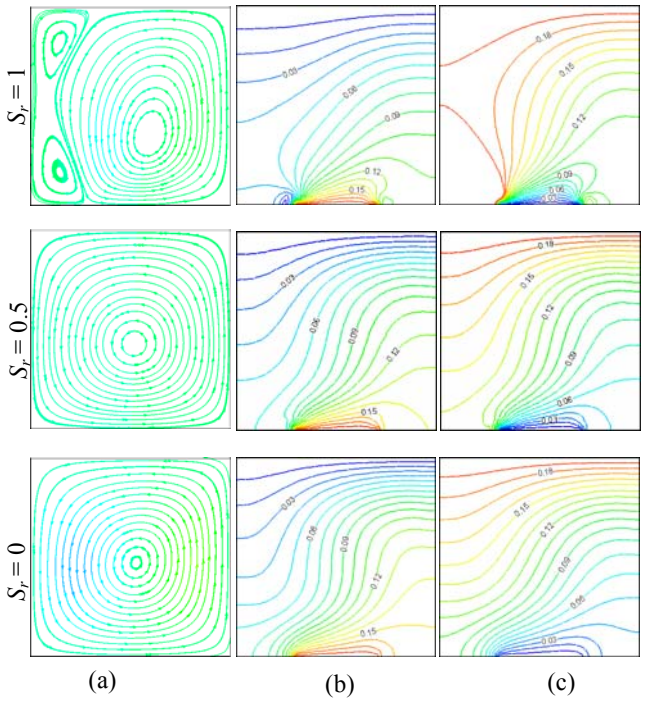


Fig. 5: Effect of $S_r$ on (a) Streamlines, (b) Isotherms and (c) Concentration at $D_f$ = 0.5 and $Sc$ = 5

The effect of $D_f$ on the flow, thermal and concentration fields is presented in Fig. 6 (a) - (c) while $S_r$ = 0.5 and $Sc$ = 5. A primary anticlockwise recirculation cell occupying the whole cavity is found for the absence of the Dufour coefficient ($D_f$). The fluid rises along the right wall and falls along the left wall. The size of the inner vortex of this cell becomes larger with the increasing of the Dufour coefficient. The strength of the flow circulation, the thermal current and concentration activities are much more activated with escalating $D_f$. Increasing $D_f$, the temperature and concentration lines at the middle part of the enclosure become vertical whereas initially they are almost horizontal. Due to rising values of $D_f$, the temperature and concentration distributions become distorted resulting in an increase in the overall heat and mass transfer. It is worth noting that as the Dufour coefficient increases, the thickness of the thermal boundary layer near the horizontal surfaces rises which indicates a steep temperature and concentration gradients. Hence, an increase in the overall heat and mass transfer within the cavity is observed.

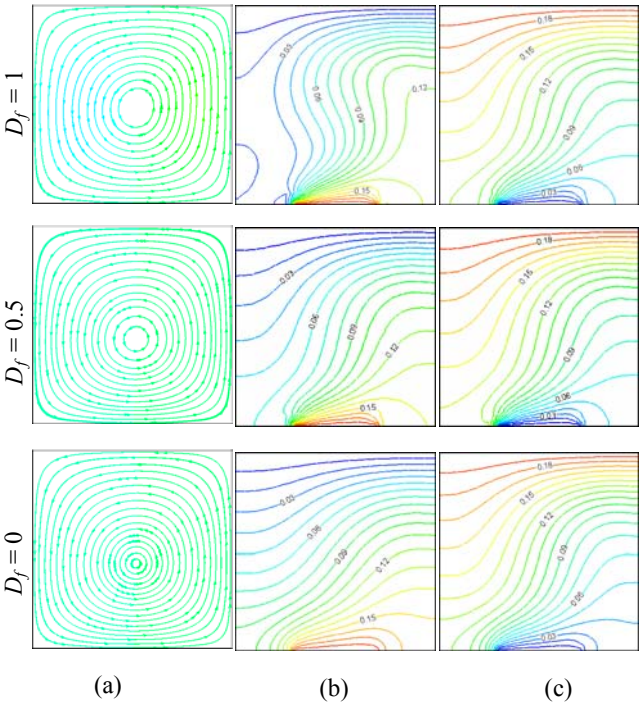


Fig. 6: Effect of $D_f$ on (a) Streamlines, (b) Isotherms and (c) Concentration at $S_r$ = 0.5 and $Sc$ = 5

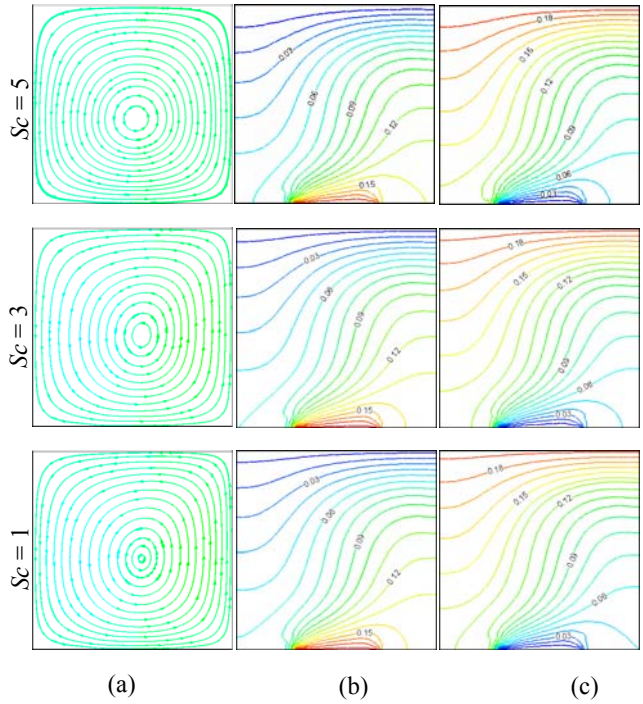


Fig. 7: Effect of $Sc$ on (a) Streamlines, (b) Isotherms and (c) Concentration at $D_f$ = $S_r$ = 0.5

The results are presented in terms of fluid flow, heat and mass transfer for various Schmidt number $Sc$ in Fig. 7(a)–(c). In this figure we find that the fluid flow covers the entire cavity at the lowest value of $Sc$. The streamlines have no significant change due to rising $Sc$ except the core of the vortex becomes slightly larger. The nature of streamlines takes horizontal pattern from vertical with the increasing of

the Schmidt number. For all values of Schmidt number, isotherms and iso-concentrations are almost similar to the active parts of the partially heated chamber. As *Sc* enhances from 1 to 5, the isotherms and iso-concentrations contours tend to get affected considerably.

The average Nusselt (*Nu*) and Sherwood (*Sh*) numbers, average temperature ($\theta_{av}$) and concentration ($C_{av}$) along with the Soret coefficient ($S_r$) are depicted in Fig. 8 (i)-(ii). It is seen from Fig. 8 (i) that *Nu* enhances gradually whereas *Sh* remains almost invariant for mounting $S_r$. Consequently Fig. 8 (ii) shows that ($\theta_{av}$) devalues and ($C_{av}$) rises sequentially for all values of Soret coefficient $S_r$.

Fig. 9 (i)-(ii) shows the mid-height horizontal and vertical velocity profiles inside the chamber for different $S_r$ effect. It is observed that the fluid particle moves with greater velocity for the absence of Soret coefficient $S_r$. The waviness devalues for higher values of $S_r$.

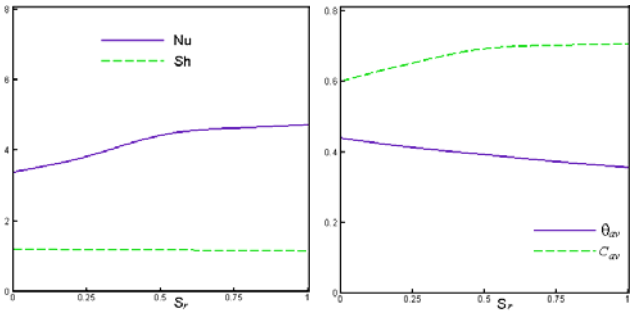


(i) (ii)

Fig. 8: Effect of $S_r$ on (i) *Nu* and *Sh* and (ii) $\theta_{av}$ and $C_{av}$ at $D_f = 0.5$ and $Sc = 5$

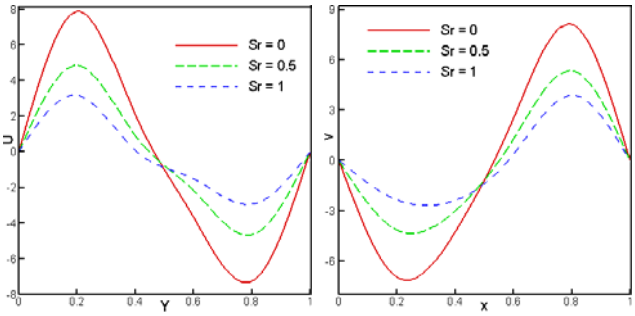


(i) (ii)

Fig. 9: Mid height (i) horizontal and (ii) vertical velocities for different $S_r$ with $D_f = 0.5$ and $Sc = 5$

Fig. 10 (i)-(ii) displays the mean Nusselt and Sherwood numbers, average temperature ($\theta_{av}$) and concentration ($C_{av}$) for the effect of Dufour coefficient $D_f$. Both *Nu* and *Sh* grow up for varying $D_f$. The rate of heat transfer is found to be more effective than the mass transfer rate. On the other hand, $\theta_{av}$ and $C_{av}$ has notable changes with different values of $D_f$. The value of mean concentration is always higher than that of average temperature at a particular value of Dufour coefficient.

The *U* and *V* velocities at the middle of the cavity for various $D_f$ are depicted in Fig. 11 (i)-(ii). A small variation in velocity is found due to changing $D_f$. Some perturbations are seen in the horizontal velocity graph for $D_f = 0$ and in the vertical velocity profile for $D_f = 1$.

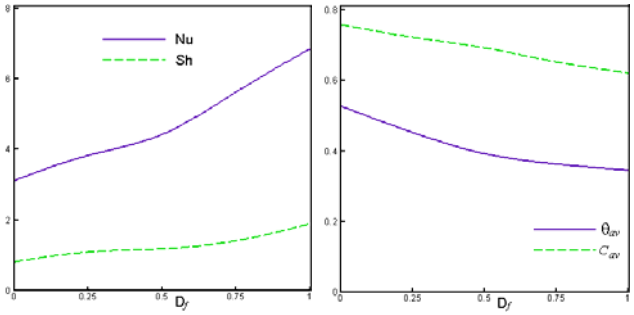


(i) (ii)

Fig. 10: Effect of $D_f$ on (i) *Nu* and *Sh* and (ii) $\theta_{av}$ and $C_{av}$ at $S_r = 0.5$ and $Sc = 5$

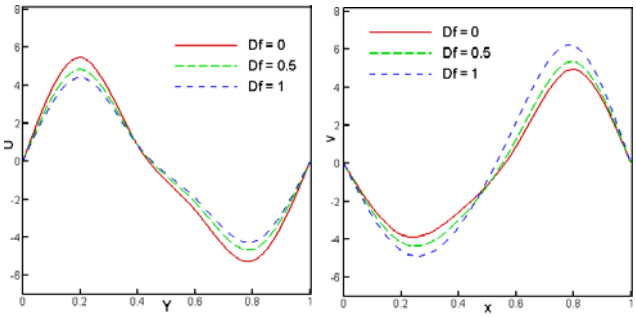


(i) (ii)

Fig. 11: Mid height (i) horizontal and (ii) vertical velocities for different $D_f$ at $S_r = 0.5$ and $Sc = 5$

The average Nusselt (*Nu*) and Sherwood (*Sh*) numbers, average temperature ($\theta_{av}$) and concentration ($C_{av}$) along with the Schmidt number (*Sc*) are depicted in Fig. 12 (i)-(ii). It is seen from Fig. 12 (i) that for mounting *Sc*, both *Nu* and *Sh* enhance steadily. The rates of heat and mass transfer rise 12% and 10% respectively for the variation of *Sc* number. This is well known that heat transfer rate is more effective than mass transfer rate and it is verified for the present study. Consequently Fig. 12 (ii) shows that ($\theta_{av}$) and ($C_{av}$) lessen slowly for all Schmidt number.

Fig. 13 (i)-(ii) shows the mid-height *Y-U* and *X-V* velocity distributions inside the chamber for the effect of *Sc*. No significant variation is shown in velocities with different *Sc* by the Fig.13. But the fluid particle moves with comparatively greater velocity for the highest Schmidt number *Sc*.

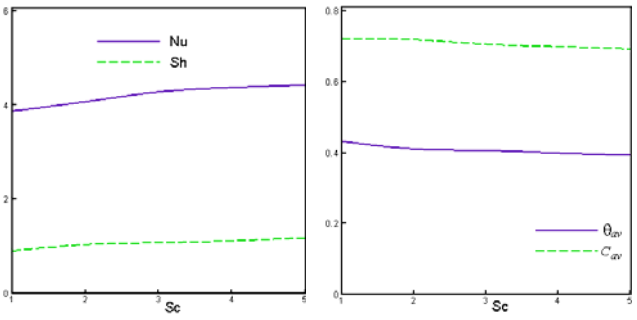


(i) (ii)

Fig. 12: Effect of *Sc* on (i) *Nu* and *Sh*, (ii) $\theta_{av}$ and $C_{av}$ at $D_f = S_r = 0.5$

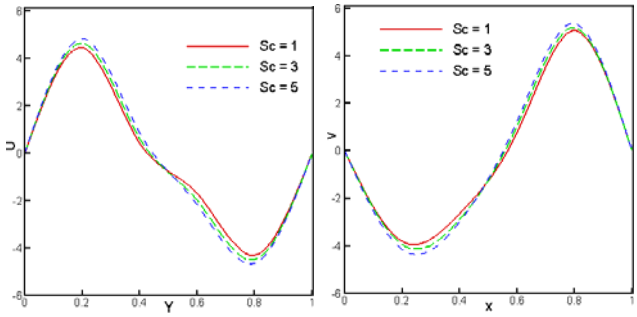


(i) (ii)

Fig. 13: Mid height (i) horizontal and (ii) vertical velocities for different *Sc* at $D_f = S_r = 0.5$

## 5. CONCLUSION

The influence of nanoparticles on natural convection boundary layer flow inside a square cavity with water-$Al_2O_3$ nanofluid is accounted. Various Soret-Dufour coefficients and Schmidt number have been considered for the flow, temperature and concentration fields as well as the heat and mass transfer rate, horizontal and vertical velocities at the middle height of the enclosure while *Pr*, *Ra* and $\phi$ are fixed at 6.2, $10^4$ and 5% respectively. The results of the numerical analysis lead to the following conclusions:

- The structure of the fluid streamlines, isotherms and iso-concentrations within the chamber is found to significantly depend upon the Soret-Dufour coefficients and Schmidt number.
- The $Al_2O_3$ nanoparticles with the highest $S_r$, $D_f$ and *Sc* is established to be most effective in enhancing performance of heat transfer rate than the rate of mass transfer.
- Greater variation is observed in velocities at a particular point for the changes of $S_r$ with compared to that of $D_f$ and *Sc*.
- Average concentration is higher than average temperature inside the chamber for the pertinent parameters.

Overall the analysis also defines the operating range where water-$Al_2O_3$ nanofluid can be considered effectively in determining the level of heat and mass transfer augmentation.

## 6. REFERENCES


[1] A. Bahloul, N. Boutana, P. Vasseur, Double-diffusive and Soret-induced convection in a shallow horizontal porous layer, *J. Fluid Mech.*, vol. 491, pp. 325–352, 2003.

[2] N. Nithyadevi, R.J. Yang, Double diffusive natural convection in a partially heated enclosure with Soret and Dufour effects. *Int. J. Heat and Fluid Flow*, vol. 30, pp. 902–910, 2009.

[3] I. Sezai, A.A. Mohamad, Double diffusive convection in a cubic enclosure with opposing temperature and concentration gradients, *Phys. Fluids*, vol. 12, pp. 2210–2223, 2000.

[4] S. Sivasankaran, P. Kandaswamy, Double diffusive convection of water in a rectangular partitioned enclosure with temperature dependent species diffusivity, *Int. J. Fluid Mech. Res.*, vol. 33, pp. 345–361, 2006.

[5] S. Sivasankaran, P. Kandaswamy, Double diffusive convection of water in a rectangular partitioned enclosure with concentration dependent species diffusivity, *J. Korean Soc. Industrial Appl. Math.*, vol. 11, pp. 71–83, 2007.

[6] A. Mansour, A. Amahmid, M. Hasnaoui, M. Bourich, Multiplicity of solutions induced by thermosolutal convection in a square porous cavity heated from below and submitted to horizontal concentration gradient in the presence of Soret effect, *Num. Heat Trans.*, vol. 49, pp. 69–94, 2006.

[7] F. Joly, P. Vasseur, G. Labrosse, Soret-driven thermosolutal convection in a vertical enclosure, *Int. Commun. Heat Mass Trans.*, vol. 27, pp. 755–764, 2000.

[8] J.K. Platten, The Soret effect: a review of recent experimental results, *J. Appl. Mech.*, vol. 73, pp. 5–15, 2006.

[9] M.K. Patha, P.V.S.N. Murthy, G.P.R. Sekhar, Soret and Dufour effects in a non-darcy porous medium, *J. Heat Trans.*, vol. 128, pp. 605–610, 2006.

[10] H.F. Oztop, Natural convection in partially cooled and inclined porous rectangular enclosures, *Int. J. Thermal Sci.*, vol. 46, pp. 149–156, 2007.

[11] R.L. Frederick, F. Quiroz, On the transition from conduction to convection regime in a cubical enclosure with a partially heated wall, *Int. J. Heat Mass Trans.*, vol. 44, pp. 1699–1709, 2001.

[12] B. Erbay, Z. Altac, B. Sulus, Entropy generation in a square enclosure with partial heating from a vertical lateral wall, *Heat Mass Trans.*, vol. 40, pp. 909–918, 2004.

[13] N. Nithyadevi, P. Kandaswamy, S. Sivasankaran, Natural convection in a square cavity with partially

active vertical walls: time periodic boundary condition, *Math. Prob. Eng.*, pp.1–16, 2006.

[14] N. Nithyadevi, P. Kandaswamy, J. Lee, Natural convection in a rectangular cavity with partially active side walls, *Int. J. Heat Mass Trans.*, vol. 50, pp. 4688– 4697, 2007.

[15] P. Kandaswamy, S. Sivasankaran, N. Nithyadevi, Buoyancy-driven convection of water near its density maximum with partially active vertical walls, *Int. J. Heat Mass Trans.*, vol. 50, pp. 942–948, 2007.

[16] H.F. Oztop, E. Abu-Nada, Numerical study of natural convection in partially heated rectangular enclosures filled with nanofluids, *Int. J. of Heat and Fluid Flow*, vol. 29, pp. 1326–1336, 2008.

[17] A. Rouboa, A. Silva, A.J. Freire, A. Borges, J. Ribeiro, P. Silva, J.L. Alexandre, Numerical analysis of convective heat transfer in nanofluid, *AIP Conference Proceedings*, 1048, pp. 819–822, 2008.

[18] J.A. Esfahani and V. Bordbar, Double Diffusive Natural Convection Heat Transfer Enhancement in a Square Enclosure Using Nanofluids, *J. of Nanotechnology in Engg. and Medicine*, vol. 2, no. 2, 021002, 2011, doi:10.1115/1.4003794.

[19] R.S.R. Gorla, A.J. Chamkha, A.M. Rashad, Mixed convective boundary layer flow over a vertical wedge embedded in a porous medium saturated with a nanofluid: Natural Convection Dominated Regime, *Nanoscale Research Letters*, vol. 6, pp. 207, 2011, doi:10.1186/1556-276X-6-207.

[20] A.V. Kuznetsov, D.A. Nield, Double-diffusive natural convective boundary-layer flow of a nanofluid past a vertical plate, *Int. J. of Thermal Sciences*, vol. 50, no. 5, pp. 712-717, 2011.

[21] D.A. Nield, A.V. Kuznetsov, The onset of double-diffusive convection in a nanofluid layer, *Int. J. of Heat and Fluid Flow*, vol. 32, no. 4, pp. 771-776, 2011.

[22] D A Nield, A V Kuznetsov, The Cheng–Minkowycz problem for the double-diffusive natural convective boundary layer flow in a porous medium saturated by a nanofluid, *Int. J. of Heat and Mass Transfer* 54, pp. 374–378, 2011.

[23] D. Pal, H. Mondal, Effects of SoretDufour, chemical reaction and thermal radiation on MHD non-Darcy unsteady mixed convective heat and mass transfer over a stretching sheet, *Commu. in Nonlinear Science and Num. Simulation*, vol. 16, no. 4, pp. 1942–1958, 2011.

[24] K.C. Lin, A. Violi, Natural convection heat transfer of nanofluids in a vertical cavity: Effects of non-uniform particle diameter and temperature on thermal conductivity, *Int. J. of Heat and Fluid Flow*, vol. 31, pp. 236–245, 2010.

[25] H. Saleh, R. Roslan, I. Hashim, Natural convection heat transfer in a nanofluid-filled trapezoidal enclosure, *Int. J. of Heat and Mass Transfer*, vol. 54, pp. 194–201, 2011.

[26] H.C. Brinkman, The viscosity of concentrated suspensions and solution, *J. Chem. Phys.*, vol. 20, pp. 571–581, 1954.

[27] J.C. Maxwell-Garnett, Colours in metal glasses and in metallic films, *Philos. Trans. Roy. Soc. A*, vol. 203, pp. 385–420, 1904.

[28] C. Taylor, P. Hood, A numerical solution of the Navier-Stokes equations using finite element technique, *Computer and Fluids*, vol. 1, pp. 73–89, 1973.

[29] P. Dechaumphai, *Finite Element Method in Engineering*, 2nd ed., Chulalongkorn University Press, Bangkok, 1999.

[30] T. Basak, S. Roy, I. Pop, Heat flow analysis for natural convection within trapezoidal enclosures based on heatline concept, *Int. J. Heat Mass Transfer*, vol. 52, pp. 2471–2483, 2009.

## 7.NOMENCLATURES

| | |
|---|---|
| $c$ | Dimensional concentration (kg m$^{-3}$) |
| $C$ | Non-dimensional concentration |
| $C_p$ | Specific heat at constant pressure (kJ kg$^{-1}$ K$^{-1}$) |
| $C_s$ | Concentration susceptibility |
| $D$ | Solutal diffusivity (m$^2$ s$^{-1}$) |
| $D_f$ | Dufour parameter, $D_f = \left(\frac{D}{\nu}\right)_f \frac{k_{Tf}\left(C_h - C_c\right)}{C_s C_p \left(T_h - T_c\right)}$ |
| $g$ | Gravitational acceleration (m s$^{-2}$) |
| $h$ | Local heat transfer coefficient (W m$^{-2}$ K$^{-1}$) |
| $k$ | Thermal conductivity (W m$^{-1}$ K$^{-1}$) |
| $K_T$ | Thermal diffusion ratio |
| $L$ | Lengh of the enclosure (m) |
| $Nu$ | Nusselt number, $Nu = hL/k_f$ |
| $Pr$ | Prandtl number, $Pr = \nu_f / \alpha_f$ |
| $Sc$ | Schmidt number, $Sc = \left(\frac{\nu}{D}\right)_f$ |
| $Sh$ | Sherwood number, $Sh = hL/k_f$ |
| $S_r$ | Soret parameter, $S_r = \left(\frac{D}{\nu}\right)_f \frac{k_{Tf}\left(T_h - T_c\right)}{T_m \left(C_h - C_c\right)}$ |
| $Ra$ | Rayleigh number, $Ra = \frac{g\beta_f L^3 \left(T_h - T_c\right)}{\nu_f \alpha_f}$ |
| $T$ | Dimensional temperature ($^o$K) |
| $u, v$ | Dimensional $x$ and $y$ components of velocity (ms$^{-1}$) |
| $U, V$ | Dimensionless velocities, $U = uL/\nu_f$, $V = vL/\nu_f$ |
| $X, Y$ | Dimensionless coordinates, $X = x/L, Y = y/L$ |
| $x, y$ | Dimensional coordinates (m) |

***Greek Symbols***

| | |
|---|---|
| $\alpha$ | Fluid thermal diffusivity (m$^2$ s$^{-1}$) |
| $\beta$ | Thermal expansion coefficient (K$^{-1}$) |
| $\phi$ | Nanoparticles volume fraction |

| | |
|---|---|
| $\theta$ | Dimensionless temperature, $\theta = \left(T - T_c\right) / \left(T_h - T_c\right)$ |
| $\mu$ | Dynamic viscosity (N s $m^{-2}$) |
| $v$ | Kinematic viscosity ($m^2$ $s^{-1}$) |
| $\rho$ | Density (kg $m^{-3}$) |

***Subscripts***

| | |
|---|---|
| *av* | average |
| *c* | cold |
| *f* | fluid |
| *h* | hot |
| *m* | mean |
| *nf* | nanofluid |
| *s* | solid particle |